INTERNATIONAL JOURNAL FOR NUMERICAL METHODS IN FLUIDS, VOL. 6, 197–218 (1986)

SIMULATION OF FORMING PROCESSES BY FEM WITH A BINGHAM FLUID MODEL

M. BERCOVIER

Department of Computer Science, The Hebrew University of Jerusalem, 91904 Jerusalem, Israel

M. ENGELMAN

Department of Mathematics, IIT, Chicago, Ill., U.S.A.

M. FORTIN

Department of Mathematics, Universite Laval, Quebec, G1K 7P4, Canada

AND

N. GOLDBERGER

Department of Computer Science, The Hebrew University of Jerusalem, 91904 Jerusalem, Israel

SUMMARY

We model the forming process as a fluid flow. A finite element program, FIDAP, which analyses flow problems, was used to calculate velocity and strain rates at points throughout the material during the deformation process. This allows predictions to be made on the shape and quality of the resulting part. The stress–strain relation we used models the plastic flow of metals (Bingham fluids). The FEM approximation of such a fluid is tested by comparing results for a simple analytical example. In forming processes provision must be made for friction between dye and workpiece, and the program was modified accordingly. Two classical ring forming simulations are compared to published results.

KEY WORDS Bingham Fluids Forming Process Non-Newtonian Flows Finite Elements

INTRODUCTION

Modelling of forming processes by a Bingham fluid flow model using a finite element method has been introduced by Lee and Kobayashi[1] and Zienkiewicz and Godbole,[2] and numerous special purpose programs have been developed and tested.[3] More references on the subject can be found in Reference 4. Starting from Reference 2 most FEM methods based on such a formulation use a reduced constraint penalty method to handle the incompressibility constraint. This is usually done by implementing a reduced integration scheme in computing the volume deformation energy. This approach introduces numerical errors, and the consistent definition of a reduced constraint formulation can be found in Reference 5 or 6. Proper definitions of the penalty and reduced constraint method will avoid 'locking' situations as well as spurious pressures. Such an approach is the basis of the general fluid flow program FIDAP.[7] Our aim

0271–2091/86/040197–22$11.00

Received 5 July 1985
Revised 1 October 1985

was to use this program (and extend it) for the simulation of forming processes. For evaluation purposes we wanted to be able to compute the error in our computations. First we give in detail the construction of a closed-form solution first published in Reference 8. Such a solution can be useful to anyone testing Bingham fluid flow codes. We then compare computed and analytical results.

Since friction between dye and workpiece is a major design parameter in the forming process a friction element is introduced and implemented in the code. Using this friction element two simple classical examples of ring forming are given and compared to previously published results. Examples of actual dye forming simulations will appear elsewhere. Notations are given in Appendix I.

PHYSICAL AND MATHEMATICAL MODEL

Equations of motion and assumptions

In the following, Cartesian tensor notation will be used with summation over repeated indices implied: u_i is the velocity component in the x_i direction; $D_{ij} = \frac{1}{2}(u_{i,j} + u_{j,i})$ is the strain rate tensor and σ_{ij} are the components of the stress tensor:

$$\sigma_{ij} = -P\delta_{ij} + \tau_{ij}, \tag{1}$$

where P is the hydrostatic pressure—the spherical part of the stress tensor—and τ_{ij} is the deviatoric stress tensor.

It is assumed that thermal effects are negligible and the fluid is homogeneous, isotropic and incompressible. The following equations of motion are obtained.

From conservation of momentum,

$$\frac{\rho \partial u_i}{\partial t} + u_j u_{i,j} = f_i + \sigma_{ij,j}. \tag{2}$$

Conservation of the moment of momentum implies the symmetry of the stress tensor, so $\sigma_{ij} = \sigma_{ji}$.

The continuity equation from conservation of mass, for an incompressible fluid is

$$u_{i,i} = 0. \tag{3}$$

Constitutive relations for Bingham and plastic flow

The relationship between the strain rate tensor and the deviatoric stress tensor for a Bingham fluid is defined as follows:[9]

$$\tau_{ij} = (g/D_{\text{II}}^{1/2} + 2\mu)D_{ij}, \tag{4}$$

where $D_{\text{II}} = \frac{1}{2}D_{ij}D_{ij}$ is the second invariant of the strain rate tensor; μ is the viscosity of the Bingham fluid and g is the yield limit (threshold of plasticity). This is defined for $D_{\text{II}} \neq 0$.

To invert the relation τ_{II}, the second invariant of the deviatoric stress tensor, is needed.

$$\tau_{\text{II}} = \tfrac{1}{2}\tau_{ij}\tau_{ij} = D_{\text{II}}(g/D_{\text{II}}^{1/2} + 2\mu)^2 = (g + 2\mu D_{\text{II}}^{1/2})^2. \tag{5}$$

Hence

$$\tau_{\text{II}} \geqslant g^2. \tag{6}$$

In this case (4) can be inverted. From (5):

$$D_{\mathrm{II}}^{1/2} = (\tau_{\mathrm{II}}^{1/2} - g)/2\mu, \tag{7}$$

$$D_{ij} = \frac{\tau_{ij} D_{\mathrm{II}}^{1/2}}{g + 2\mu D_{\mathrm{II}}^{1/2}} = \frac{\tau_{ij}(\tau_{\mathrm{II}}^{1/2} - g)}{2\mu(\tau_{\mathrm{II}}^{1/2})}.$$

The constitutive laws are therefore

$$\left.\begin{aligned} &\text{when } \tau_{\mathrm{II}} < g^2 \\ &\qquad D_{ij} = 0, \\ &\text{when } \tau_{\mathrm{II}} \geqslant g \\ &\qquad D_{ij} = (1 - g/\tau_{\mathrm{II}}^{1/2})\tau_{ij}/2\mu, \\ &\text{or} \\ &\qquad \tau_{ij} = (g/D_{\mathrm{II}}^{1/2} + 2\mu)D_{ij}. \end{aligned}\right\} \tag{8}$$

When a body is replaced under small loading forces it deforms but regains its original shape when the stresses are released. This is elastic deformation. When the loading forces are increased further, they can reach a point at which the body will not return to its original shape—this is plastic deformation, and occurs in metal forming processes.

Von Mises suggested a criterion to determine when material would reach this stage. As long as the second invariant of stress (τ_{II}) remains less than a characteristic value for the material, k^2, deformation will be elastic. When τ_{II} reaches k^2, the material is at yield, and if no strain hardening occurs, τ_{II} will not exceed k^2.

In order to evaluate k in terms of yield stress in a uniaxial tensile test, τ_{II} can be written in terms of σ_{ij}:

$$\begin{aligned} \tau_{\mathrm{II}} &= \tfrac{1}{6}\{(\sigma_{11} - \sigma_{22})^2 + (\sigma_{22} - \sigma_{33})^2 + (\sigma_{33} - \sigma_{11})^2\} + \sigma_{12}^2 + \sigma_{23}^2 + \sigma_{31}^2 \\ &= k^2. \end{aligned} \tag{9}$$

In a uniaxial tensile test, $\sigma_{11} = \sigma_0$, the tension at which yield is reached, and all other σ_{ij} are equal to zero.

Hence from (9), at yield

$$\tau_{\mathrm{II}} = k^2 = \sigma_0^2/3, \tag{10}$$

$$k = \sigma_0/\sqrt{3}. \tag{11}$$

A simplified description of the stress–strain relation for metals in the plastic range is given by St. Venant:

$$D_{ij} = \lambda \tau_{ij},$$

where λ is a function of strain rates. Hence

$$D_{\mathrm{II}} = \lambda^2 \tau_{\mathrm{II}}. \tag{12}$$

Using the Von Mises yield criterion (10)

$$D_{\mathrm{II}} = \lambda^2 k^2,$$

$$\lambda = \pm D_{\mathrm{II}}^{1/2}/k,$$

so that

$$D_{ij} = (D_{\mathrm{II}}^{1/2}/k)\tau_{ij}; \quad \tau_{ij} = (k/D_{\mathrm{II}}^{1/2})D_{ij} \qquad \text{for} \quad \tau_{\mathrm{II}} \geqslant k^2. \tag{13}$$

A material obeying (13) is known as a Von Mises material and in effect satisfies the Bingham relation (8) with $\mu = 0$. Note that the material is rigidly perfectly plastic—there is no deformation in the elastic zone, and no deformation until (10) is reached. The strain is therefore only plastic. The hydrostatic pressure P is not determined and does not affect yielding and flow.

Hence Von Mises flow can be modelled by a Bingham fluid with $\mu = 0$, and

$$g = k = \sigma_0/\sqrt{3}. \tag{14}$$

In fact a small positive μ was used, since solution existence, uniqueness and convergence results are valid for non-zero μ.

In the computer program FIDAP, τ_{II} and D_{II}, determining the Bingham relation, are defined as follows:

$$\tau'_{\text{II}} = \tau_{ij}\tau_{ij} = \tfrac{1}{2}\tau_{\text{II}}$$
$$D'_{\text{II}} = D_{ij}D_{ij} = \tfrac{1}{2}D_{\text{II}}$$

where $'$ means 'as defined in FIDAP'. Hence $\tau'_{ij} = (g/2D_{\text{II}})^{1/2})D_{ij}$.

Therefore the g chosen for use with FIDAP was $\sqrt{(2k)}$ so that (13) would be fulfilled.

Friction

In the forming process, there is frictional resistance encountered to the motion between the dye and material. It results in a shear stress on the surface of the material. Various models are used to describe this stress. The one which was applied here was that of a constant friction factor, m:

$$\tau_{ij} = m\sigma_0/\sqrt{3}. \tag{15}$$

m is constant for given dye and material under constant surface and temperature conditions, and is considered independent of velocity. Since the maximum shear a material can stand from the Von Mises yield criterion (10) is $\sigma_0/\sqrt{3}, 0 \leqslant m \leqslant 1$. Further details of the implementation of friction are given in Appendix II.

Other approaches have been suggested, such as a non-linear variable stiffness element method; see Reference 10 and references therein.

Abstract formulation of problem, variational representation

Given a bounded domain Ω of $\mathbb{R}^2$, $\Gamma_1 \cup \Gamma_2$ its boundary, meas $(\Gamma_1) \neq 0$, the solution is required to equations (2) and (3) where the constitutive relations are given by (1) and (8), and boundary conditions are

$$u_i = 0 \quad \text{on} \quad \Gamma_1. \tag{16}$$

This represents fluid flow in the interior of Ω and will be called *problem P1*.

Restricting discussion to the two-dimensional problem, the following space is used (see, for instance, Reference 9 for definitions):

$$V = \{u \in (H^1)(\Omega)^2), \quad \operatorname{div} v = 0; \quad u_{i|\Gamma_1} = 0\}.$$

The following forms are defined for vector fields u, v, w on Ω:

$$a(u, v) = 2\int_\Omega D_{ij}(u)D_{ij}(v) : V \times V \to \mathbb{R}, \tag{17}$$

$$j(v) = 2\int_{\Omega} (D_{\mathrm{II}}(v))^{1/2}\mathrm{d}x, \tag{18}$$

$$c(u, v, w) = \int_{\Omega} u_i v_{j,i} w_j \mathrm{d}x : V \times V \times V \to \mathbb{R}. \tag{19}$$

Given $f \in L^2(0, T, V')$, it can be shown[9] that the solution to problem P1 is also the solution to the following variational problem:

$$\left(\frac{\partial u}{\partial t}, v\right) + \mu a(u, v) + c(u, u, v) + g(j'(u), v) = f(v), \tag{20}$$

where

$$g(j'(u), v) = \int_{\Omega} D_{\mathrm{II}}(u)^{-1/2} D_{ij}(u) D_{ij}(v)\,\mathrm{d}x. \tag{21}$$

It is not always easy to work in divergence-free spaces, and therefore it is useful to consider an alternative formulation of problem P1.

The following spaces are defined:

$$X = (H_0^1(\Omega))^2,$$
$$M = L^2(\Omega)/\mathbb{R}$$

and the bilinear form $b(.,.): X \times M \to \mathbb{R}$

$$b(u, q) = -(q, \mathrm{div}\, u). \tag{22}$$

Discussion will be limited for simplicity to the stationary problem, where the $\partial u/\partial t$ term is omitted. Then under the following conditions.

(i) α (.,.) is elliptic on V, i.e. there exists a constant $\alpha > 0$ such that

$$a(v, v) \geqslant \alpha \| v \|_X^2, \quad \forall v \in V. \tag{23}$$

(ii) The Brezzi–Babuska hypothesis holds, i.e.

$$\sup_{v \in X - \{0\}} \frac{|b(v, q)|}{\| v \|_X} \geqslant \beta \| q \|_M. \tag{24}$$

Problem P1 is equivalent to

Find $(u, p) \in X \times M$ such that

$$\left.\begin{aligned} &\mu a(u, v) + b(v, p) + c(u, u, v) + g(j'(u), v) = f(v), \\ &b(u, q) = 0 \end{aligned}\right\} \quad \forall (v, q) \in X \times M. \tag{25}$$

(Problem P2).

In effect, p here is a Lagrange multiplier associated with the constraint $b(u, q) = 0$.

For numerical solution of problem P2, there are various difficulties—the incompressibility constraint, the non-linear term $c(u, v, w)$ and the fact that the functional $j(v)$ is not differentiable.

To help overcome these difficulties a perturbed problem is introduced, and it is 'linearized' to

$$\left.\begin{aligned} &\mu a(u_\varepsilon, v) + b(p_\varepsilon, v) + \lambda c(u_\varepsilon, u_\varepsilon, v) + g(j'(u_\varepsilon), v) = f(v), \\ &\varepsilon(p_\varepsilon, q) - b(q, u_\varepsilon) = 0, \end{aligned}\right\} \quad \forall (v, q) \in X \times M. \tag{26}$$

(Problem P3).

p_ε can be eliminated, so that the perturbation can be seen as a penalty function on the original problem, to give

Find $u_\varepsilon \in X$ such that

$$\mu a(u_\varepsilon v) + \frac{1}{\varepsilon}\int_\Omega \nabla u_\varepsilon \nabla v\, dx + \lambda c(u_\varepsilon, u_\varepsilon, v) + g(j'(u_\varepsilon), v) = f(v), \quad \forall v \in X. \tag{27}$$

(Problem P4).

In Reference 11 it was shown that under the following condition:

$$\lambda c[f]_* \leqslant \delta < 1,$$

where c and $[f]_*$ are given by

$$c(u, v, w) \leqslant ca(u, v)^{1/2} a(v, v)^{1/2} a(w, w)^{1/2}, \tag{28}$$

$$[f]_* = \sup_{v \in X - \{0\}} \frac{|(f, v)|}{\|v\|}, \tag{29}$$

problem P3 has a unique solution and

$$\|u - u_\varepsilon\|_X \leqslant c(f, \Omega)\sqrt{\varepsilon}. \tag{30}$$

In numerical work, to prevent the problem of $D_{\mathrm{II}} = 0$, the following formulation is used,[12] which is derived from (27), and for which the same error estimate holds:

$$\mu a(u_\varepsilon, v) + c(u_\varepsilon, u_\varepsilon, v) + g\int_\Omega \frac{D_{ij}(u_\varepsilon) D_{ij}(v)}{(D_{\mathrm{II}}(u_\varepsilon) + \eta^2)^{1/2}}\, \mathrm{d}x + \frac{1}{\varepsilon}\int_\Omega \nabla u_\varepsilon \nabla v\, \mathrm{d}x = (f, v) \tag{31}$$

$a(.,.)$ is X elliptic, since

$$a(u, v) = (\mathrm{grad}\, u, \mathrm{grad}\, v). \tag{32}$$

Hence $a(v, v) = |v|^2_{1.\Omega}$, which can be a norm for X, and hence (23) is fulfilled.

Condition (24) is fulfilled by a standard result.[13] In numerical approximations it is necessary to ensure that it still holds.

Another result which can be used for numerical formulations is[9]

For (u, p) a solution of problem P2, there exist $m_{ij} \in K$ such that

$$\mu a(u, v) + b(v, p) + c(u, u, v) + g(m, D(v)) = (f, v), \quad \forall v \in X, \tag{33}$$

$$b(u, q) = 0, \quad \forall q \in M, \tag{34}$$

$$j(u) = (m, D(u)) \geqslant (n, D(u)). \quad \forall n_{ij} \in K, \tag{35}$$

where $(m, D(v))$ is defined by

$$(m, D(v)) = \int_\Omega m_{ij} D_{ij}(v)\, \mathrm{d}x. \tag{36}$$

NUMERICAL PROCEDURES

Finite elements

Nine node isoparametric quadrilaterals were used with biquadratic interpolation functions for velocity. Discontinuous pressure approximations were used for most of the problems, to enable the penalty function approach to be used, with linear interpolation for the pressure. The three pressure degrees of freedom are then the coefficients of the linear polynomial approximating the pressure on the element. The basic functions were chosen to be in the global space $\{1, x, y\}$.

It can be shown[8] that for the approximate solution (u_h, p_h) to problem P2 in the discrete spaces X_h, M_h defined by the finite element approximations above, the following error estimate holds, where (u, p) is the exact solution to problem P2:

There exist constants c_1, c_2, c_3 independent of h such that

$$\|u-u_h\|^2 \leqslant c_1 \inf_{\substack{v_h \in X_h \\ \nabla_h v_h = 0}} \|v_{h-u}\|_X^2 + c_2 g \inf_{\substack{v_h \in X_h \\ \nabla_h v_h = 0}} \|v_h - u\|_X + c_3 \inf_{q_h \in M_h} |p-q_h|^2 \tag{37}$$

(the operator ∇_h is defined in the next section).

Penalty formulation

For simplicity, the stationary equations of Stokes flow will be considered in the following.

The discretized approximation of the variational problem in finite element spaces X_h, M_h is Find $(u_h, p_h) \in X_h \times M_h$ such that

$$\mu a(u_h, v_h) - (p_h, \nabla_h, v_h) = (f, v_h), \qquad \forall v_h \in X_h, q_h \in M_h, \tag{38}$$

$$(\nabla_h u_h, q_h) = 0, \tag{39}$$

where ∇_h is the linear operator defined by

$$\nabla_h : X_h \to M_h \quad (\nabla v_h, q_h) = (\nabla_h v_h, q_h) \quad \forall (v_h, q_h) \in X_h \times M_h. \tag{40}$$

The penalty formulation of the problem is given by
Find $(u_h^\varepsilon, p_h^\varepsilon) \in X_h \times M_h$ such that

$$\mu a(u_h^\varepsilon, v_h) - (p_h^\varepsilon, \nabla_h v_h) = (f, v_h), \qquad \forall v_h \in X_h, q_h \in M_h, \tag{41}$$

$$(\nabla_h u_h^\varepsilon, q_h) = -\varepsilon (p_h^\varepsilon, q_h). \tag{42}$$

By choosing q_h so that $q_h = \nabla_h v_h, p_h^\varepsilon$ can be eliminated from (41) to give
Find $u_h \in X_h$ such that

$$\mu a(u_h^\varepsilon, v_h) + \frac{1}{\varepsilon}(\nabla_h u_h^\varepsilon, \nabla_h v_h) = (f, v_h), \qquad \forall v_h \in X_h. \tag{43}$$

The pressure is then recovered by

$$p_h^\varepsilon = -\frac{1}{\varepsilon} \nabla u_h^\varepsilon. \tag{44}$$

Use of this weaker form of the incompressibility constraint is necessary in order to ensure that the Brezzi–Babuska hypothesis (24) holds.

Here we use the consistent reduced constraint.[5] The corresponding choice of the penalty parameter ε is independent of the problem but for the dimension of the Bingham coefficient g. Our choice was to set ε of order $g \times 10^{-3}$.

Solution algorithm and method

The following algorithm is used[12] to solve problem P4 in finite element approximation space X_h, where u^0 is an initial guess, u^n the nth iterate, then u^{n+1} is computed from (dropping superscript ε)

$$\mu a(u^{n+1}, v_h) + c(u^n, u^{n+1}, v_h) + \frac{1}{\varepsilon}(\nabla_h u^{n+1}, \nabla_h v_h) \tag{45}$$

$$+ g \int_\Omega \frac{D_{ij}(u^{n+1}) D_{ij}(v_h)}{(D_{\mathrm{II}}(u^n) + \eta^2)^{1/2}} \mathrm{d}\Omega = \int_\Omega f_h v_h \mathrm{d}\Omega, \qquad \forall v_h \in X_h.$$

The iteration can be modified by defining the new u^{n+1} as

$$u^{n+1^*} = \alpha u^n + (1 - \alpha) u^{n+1}, \qquad 0 \leqslant \alpha \leqslant 1, \tag{46}$$

where α is a relaxation or acceleration factor.

Convergence

FIDAP uses two criteria to terminate iteration. Two solution variables available are the solution vector u^i (at iteration i) and the residual vector $R(u^i)$. One criterion used is that

$$\frac{\| \nabla u^i \|}{\| u^i \|} \leqslant \varepsilon_u, \qquad \text{where} \quad \nabla u^i = u^i - u^{i-1}. \tag{47}$$

This criterion is not always sufficient, and therefore a second criterion used is that

$$\frac{\| R(u^i) \|}{\| R(u^0) \|} \leqslant \varepsilon_f. \tag{48}$$

Default values for ε_u and ε_f are 0·01.

The condition for rigid flow is the one given in Reference 12.

$$D_{\mathrm{II}}^{1/2} \leqslant ch^2; \quad h = \text{element radius}, \tag{49}$$

in rigid regions of flow.

In many cases, particularly where a high friction factor was used, the solution did not approach convergence at all, and the criteria for convergence increased rather than decreased, or remained stationary. It was found that altering the iteration acceleration factor (α) (see preceding section) usually helped convergence eventually, but often many iterations were required, as the criteria increased considerably before finally decreasing to sufficiently low levels.

Another technique used to help achieve convergence was the following. FIDAP allows a number of options for determination of the initial velocity field, for the first iteration of the iterative procedure. The velocities at each node can be specified. For cases of high friction, the program was first run on the mesh, with infinite friction simulated, by fixing the velocity boundary codes to eliminate the tangential degrees of freedom totally for surface nodes, so that no tangential motion at all was allowed at the dye–workpiece interface. This run converged without problem. The results obtained from this run were then used as the initial velocity field for a regular run, in which the surface nodes were free to move tangentially, too.

AN ANALYTICALLY SOLUBLE EXAMPLE OF BINGHAM FLOW

Closed form solution of problem

In Reference 8 we gave a closed form solution. Since Reference 8 is not easily accessible and contains typographical errors, we recall its construction here. We consider the flow of a Bingham fluid contained within two cylinders, with the outer cylinder rotating with constant angular speed ω. Inner and outer radii are a and b, respectively.

The solution is given by $u=(u_r, u_\theta)$ where u_r is the radial and u_θ is the tangential component of velocity. Here

$$u_r = 0, \qquad \forall\, r, \theta; \quad u_\theta = u_\theta(r). \tag{50}$$

The equations of motion in cylindrical co-ordinates are given by

$$\frac{\partial \sigma_{r\theta}}{\partial r} + \frac{\sigma_{rr} - \sigma_{\theta\theta}}{r} = \frac{-u_\theta^2}{r}, \tag{51}$$

$$\frac{\partial \sigma_{r\theta}}{\partial r} + \frac{2\sigma_{r\theta}}{r} = 0. \tag{52}$$

Stress and strain are related by the Bingham relation given by (1) and (4).

From (52)

$$\sigma_{r\theta} = \tau_{r\theta} = \frac{A}{r^2}, \tag{53}$$

where A is a constant to be computed.

From (50) and the stress–strain relations

$$\begin{aligned} D_{rr} &= D_{\theta\theta} = 0, \\ \tau_{rr} &= \tau_{\theta\theta} = 0. \end{aligned} \tag{54}$$

In cylindrical co-ordinates

$$D_{r\theta} = \tfrac{1}{2} r \frac{\partial}{\partial r}\left(\frac{u_\theta}{r}\right). \tag{55}$$

Recalling that $D_{\mathrm{II}} = D_{ij} D_{ij}$, $\tau_{\mathrm{II}} = \tau_{ij}\tau_{ij}$(54) and (53) give

$$\tau_{\mathrm{II}} = \tau_{r\theta}\sqrt{2} = \frac{A\sqrt{2}}{r^2}. \tag{56}$$

From (8)

$$D_{r\theta} = \frac{1}{2\mu}\left[1 - \frac{g}{\tau_{\mathrm{II}}^{1/2}}\right]\tau_{r\theta}. \tag{57}$$

With (53 and 56)

$$\begin{aligned} D_{r\theta} &= \frac{1}{2\mu}\left[1 - \frac{g r^2}{A\sqrt{2}}\right]\frac{A}{r^2}, \\ D_{r\theta} &= \frac{1}{2\mu}\left[\frac{A}{r^2} - \frac{g}{\sqrt{2}}\right]. \end{aligned} \tag{58}$$

Hence, using (55)

$$\frac{r\partial}{\partial r}\left[\frac{u_\theta}{r}\right] = \frac{1}{\mu}\left[\frac{A}{r^2} - \frac{g}{\sqrt{2}}\right]. \tag{59}$$

Integrating from inner radius a to r:

$$\frac{u_\theta}{r} = \frac{A}{2\mu}\left[\frac{1}{a^2} - \frac{1}{r^2}\right] - \frac{g}{\mu\sqrt{2}}\ln(r/a). \tag{60}$$

There are two possible cases.

Case I. Fully viscous flow in which $\tau_{\text{II}} > g^2$ for all r. If $u_\theta/r = \omega$ on the outer radius, $r = b$, (60) gives

$$\omega = \frac{A}{2\mu}\left[\frac{1}{a^2} - \frac{1}{b^2}\right] - \frac{g}{\mu\sqrt{2}}\ln(b/a). \tag{61}$$

Hence,

$$A = 2\left[\frac{\mu\omega + \frac{g}{\sqrt{2}}\ln(b/a)}{\frac{1}{a^2} - \frac{1}{b^2}}\right]. \tag{62}$$

Substituting in (60)

$$u_\theta(r) = \frac{r}{\mu}\left[\frac{\mu\omega + \frac{g}{\sqrt{2}}\ln(b/a)}{\frac{1}{a^2} - \frac{1}{b^2}}\right]\left[\frac{1}{a^2} - \frac{1}{r^2}\right] - \frac{gr}{\mu\sqrt{2}}\ln(r/a), \tag{63}$$

as long as $\tau_{\text{II}}^{1/2} \geqslant g$, i.e.

$$A\sqrt{2}/b^2 \geqslant g. \tag{64}$$

Case II. If $A\sqrt{2}/r^2$ is not greater than g for all r, there exists an $r_0, a \leqslant r_0 \leqslant b$ such that

$$A\sqrt{2}/r_0^2 = g. \tag{65}$$

Boundary conditions are now given by

$$u_\theta(r_0) = r_0\omega, \tag{66}$$

so substituting in (60)

$$\omega = \frac{A}{2\mu}\left[\frac{1}{a^2} - \frac{1}{r_0^2}\right] - \frac{g}{\mu\sqrt{2}}\ln(r_0/a), \tag{67}$$

so that

$$A = 2\left[\frac{\mu\omega + \frac{g}{\sqrt{2}}\ln(r_0/a)}{\frac{1}{a^2} - \frac{1}{r_0^2}}\right] \tag{68}$$

and

$$
\left.\begin{aligned}
u_\theta(r) &= \frac{r}{\mu}\left[\frac{\mu\omega + \dfrac{g}{\sqrt{2}}\ln(r_0/a)}{\dfrac{1}{a^2}-\dfrac{1}{r_0^2}}\right]\left[\frac{1}{a^2}-\frac{1}{r_0^2}\right] - \frac{gr}{\mu\sqrt{2}}\ln(r/a), && \text{for} \quad a \leqslant r \leqslant r_0,\\
u_\theta(r) &= r\omega, && \text{for} \quad r_0 \leqslant r \leqslant b.
\end{aligned}\right\} \tag{69}
$$

r_0 is computed from (65)

$$
2\sqrt{2}\left[\mu\omega + \frac{g}{\sqrt{2}}\ln(r_0/a)\right] = g r_0^2\left[\frac{1}{a^2}-\frac{1}{r_0^2}\right],
$$

$$
\mu\omega + \frac{g}{\sqrt{2}}\ln(r_0/a) = \frac{g}{2\sqrt{2}}\left[\frac{r_0^2}{a^2}-1\right]. \tag{70}
$$

Given g, r_0 can be calculated numerically by successive substitutions using, from (70), (where r_0^n is the nth iterate),

$$
r_0^{n+1} = a\left[\frac{2\sqrt{2}\mu\omega}{g} + 1 + 2\ln(r_0^n/a)\right]^{1/2}. \tag{71}
$$

Alternatively, a desired r_0 can be chosen and the corresponding g calculated from the following (derived from (70)):

$$
g = \frac{2\sqrt{2}\mu\omega}{\dfrac{r_0^2}{a^2} - 2\ln(r_0/a) - 1}. \tag{72}
$$

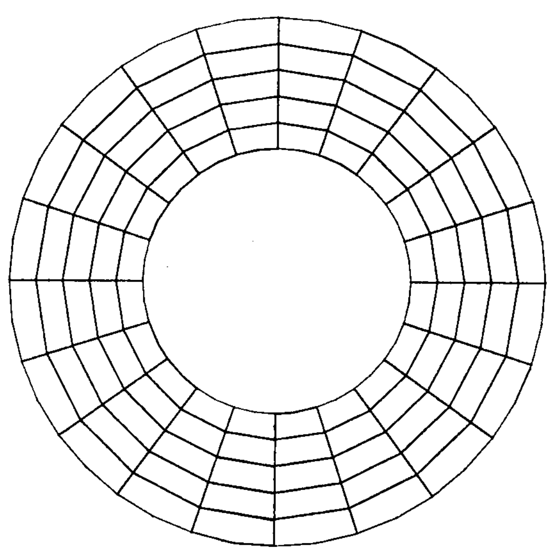

Figure 1. 'Streamline' mesh

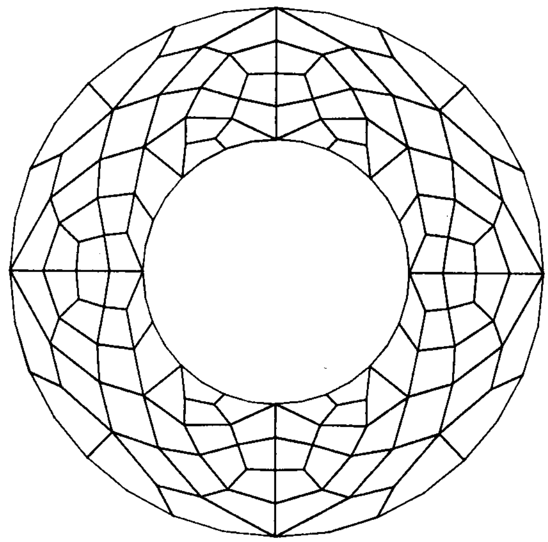

Figure 2. 'General' mesh

Numerical experiments

Numerous numerical computations were given in Reference 8; there the mesh was streamline orientated (cf. Figure 1). Here we shall consider only one case, mainly to illustrate that there is no loss of accuracy when a 'general' mesh is used (Figure 2).

For numerical computations the following values were set:

$$a = 0{\cdot}5, \quad b = 1{\cdot}0, \quad \omega = \mu = 1{\cdot}0, \quad g = 7{\cdot}1010, \quad r_0 = 0{\cdot}7375.$$

These values yield a free boundary which does not fall on a node.

Results

The numerical results on both mesh discretizations display good agreement with the theoretical solutions.

Tables I and II give for the regular discretization and the non-streamline discretization the radius vector r, and corresponding velocity and the discretization found numerically and analytically.

For the regular division velocities were symmetrical, as can be seen from Figure 3.

In both cases, the accuracy is acceptable for the number of elements used and it can be seen that the error is larger next to the boundary, where the solution is not C^1. The error in the

Table I. Velocity results, regular division

Radius, r	0·55	0·60	0·65	0·70	0·75	0·80	0·85	0·90	0·95	1.0
Numerical velocity, V_n	0·264	0·459	0·595	0·681	0·741	0·794	0·844	0·894	0·948	1.00
Analytic velocity, V_a	0·258	0·452	0·593	0·690	0·750	0·800	0·850	0·900	0·950	1.00
Error, $V_n - V_a$	0·006	0·007	0·002	−0·009	−0·009	−0·006	−0·006	−0·006	0·002	

Table II. Velocity results, non-streamline division

Radius, r	0·530	0·545	0·563	0·575	0·600	0·625	0·635	0·665	0·688	0·710	0·750	0·797	0·814	0·840	0·875	0·906	0·961	1·0
Numerical velocity, V_n	0·161	0·237	0·314	0·365	0·456	0·531	0·557	0·620	0·657	0·691	0·740	0·789	0·806	0·834	0·868	0·901	0·959	1·0
Analytic velocity, V_a	0·163	0·235	0·312	0·362	0·452	0·529	0·556	0·627	0·670	0·705	0·750	0·797	0·814	0·840	0·875	0·906	0·961	1·0
Error, $V_n - V_a$	0·002	0·002	0·002	0·003	0·004	0·002	0·001	−0·007	−0·013	−0·014	−0·010	−0·008	−0·008	−0·006	−0·007	−0·005	−0·002	—

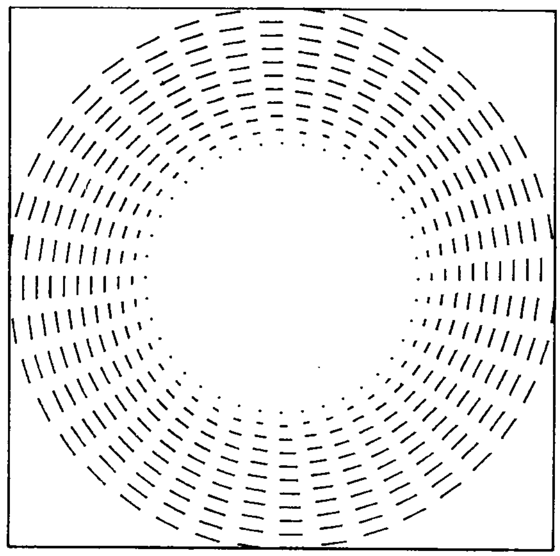

Figure 3. 'Streamline' mesh: Bingham fluid, velocity vector plot

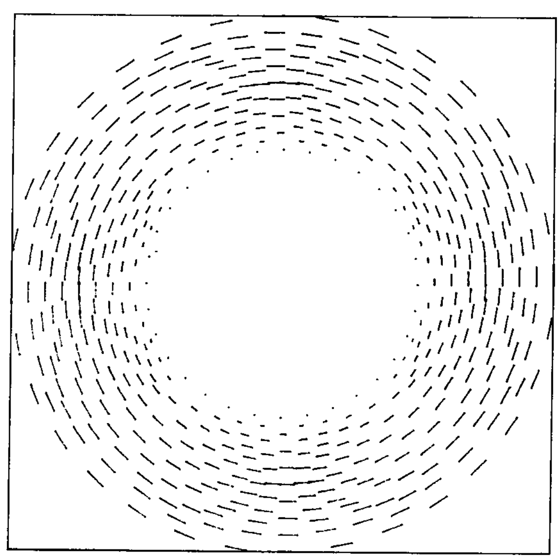

Figure 4. 'General' mesh: Bingham fluid—non-streamline division; velocity vector plot

Table III.

Node number	x co-ordinate	y co-ordinate	Radius r	Velocity
(a) $r \simeq 0.75$				
54	0·729	0·177	0·750	0·739
55	0·694	0·285	0·750	0·739
58	0·750	0·000	0·750	0·740
59	0·748	0·054	0·750	0·740
148	0·347	0·667	0·752	0·740
(b) $r = 0.587$–0.600 *(note steady increase of velocities with radius)*				
71	0·479	−0·339	0·587	0·409
50	0·480	0·341	0·589	0·416
74	0·412	0·426	0·592	0·429
29	0·536	0·270	0·600	0·456

non-streamline discretization is larger in general than with the regular discretization, but not excessively so. The error in the right zone is due to the numerical computation of

$$\int_{\Omega} \frac{D_{ij}(u)D_{ij}(v)}{(D_{\mathrm{II}}(u)+\eta^2)^{1/2}}\,\mathrm{d}\Omega.$$

The maximum error is 2 per cent.

For the non-streamline discretization, the relative symmetry of velocity results can be seen from the velocity vector plot (Figure 4), and from Table III, which gives two examples of results from different nodes with approximately the same radius vector r. The results can be seen to be very similar.

FORMING PROCESS SIMULATIONS

Ring compression example 1

Problem definition. Oh, Lahoti and Altan[3] describe the use of a finite element program, ALPID, to simulate compression of a short ring specimen. This example was tried with FIDAP to compare results and see if they were similar.

The material used for calculation was Ti-6242–0·1 Si at 1750° F. Since the experimental stress–strain rate relation could not be obtained, it was approximated from information in Reference 3 for lower temperatures, that yield strength is 450 MPa. This is equivalent to $450 \times 10^3\,\mathrm{kg\,mm^{-1}\,s^{-1}}$, for the units used (kg, mm) and gives g for use in FIDAP of 360×10^3. Some variations of this g were tried (see below).

The initial dimensions of the ring were

height = 25·4 mm (1 in.),
internal radius = 38·1 mm (1·5 in.),
outer radius = 76·2 mm (3 in.);

dye velocity was 25·4 mm/s (1 in./s) and the step size used was 4 per cent of the undeformed workpiece height. A mesh of 4 elements was used.

A series of instructions was given which ran the program, recorded the velocity vectors, changed the mesh according to the velocities calculated and drew the new mesh, and continued in this way for several stages.

Since the value of g was high, it was important to use a high penalty parameter, ε, which was taken as 10^{-9}.

Results for $m = 0{\cdot}60$. Convergence was only achieved by using an initial velocity field obtained from a simulation of infinite friction. Using this, with an iteration acceleration factor of 0·85 (i.e. changing the velocities by a relatively small amount each iteration), and a threshold velocity to reduce stress of 5 mm/s, convergence to a solution was obtained.

The solution compared with that of Oh, Lahoti and Altan, showing the neutral radius inside the inner diameter from the beginning, and convex inner and outer surfaces.

Figures 5 (a), (b) and (c) show velocity vectors initially, after 20 per cent and after 40 per cent deformation. Figures 6 (a), (b) and (c) show the mesh initially and after 20 per cent and 40 per cent deformation. It can be seen to be very similar to Oh. Lahoti and Altan's results in Figure 5 of Reference 3.

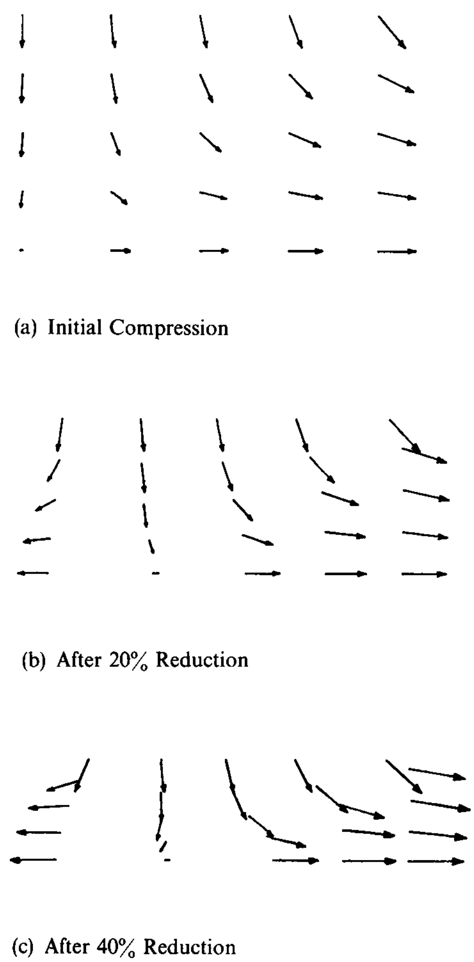

Figure 5. Ring compression: velocity vector

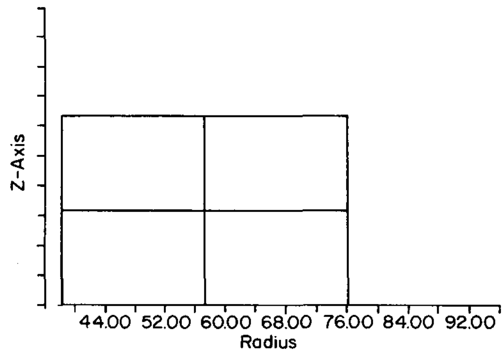

(a) Initial shape

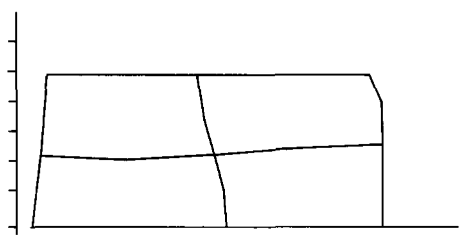

(b) After 20% Reduction

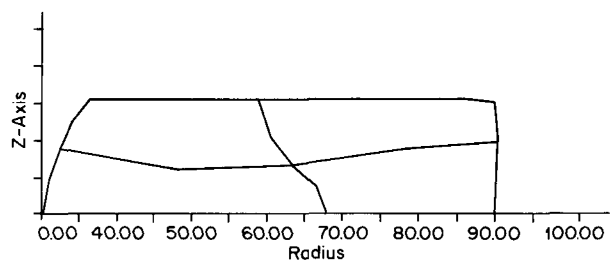

(c) After 40% Reduction

Figure 6. Ring compression: deformed shape

Ring compression example 2

Problem definition. Nagpai, Lahoti, and Altan[14] describe a deformation pattern used in an upper bound analysis of ring compression to predict velocities and strain in the metal flow. Information on internal diameters of upset forged rings can be used to indicate frictional conditions at the dye–ring interface. The examples given there were tried with FIDAP and results compared with their theoretical and experimental results.

Material used was Aluminium 1100-F upset at room temperature and 800° F (427° C). Yield strength was taken at room temperature as for O Temper Al 1100 as 34 MPa (13) equivalent to 34,000 kg $mm^{-1} s^{-1}$, giving g for use in FIDAP as 28,000. For the higher temperature, yield strength is about 11 MPa[15] giving g for FIDAP of about 8000.

Dimensions of the rings were:
heights = 36 mm and 18 mm,
outer diameter (OD) = 54 mm,
internal diameter (ID) = 27 mm;
dye velocity for a press wih 254 mm stroke at 90 strokes/min was 381 mm/s.

Assuming symmetrical deformation, as was assumed in Reference 14, the analysis was performed on rings of half the given height, with half the dye velocity, 191 mm/s.

A mesh of 15 elements was used for the thin specimen and 30 elements for the thicker specimen.

The friction factor, m, was taken from Reference 14 to be 0·52 for cold conditions and 1·0 for hot forming. Step size was 5·5 per cent of the thin ring and 2·3 per cent of the thick ring. The pressure penalty parameter was taken as 10^{-8}, since g was high. This analysis was done isothermally, and did not include heat effects. In principle, FIDAP could be used for a non-isothermal analysis.

Results for ring 6:3:4(OD:ID:height). Nagpai, Lahoti and Altan[14] found experimentally that the thicker rings buckled under both hot and cold conditions, which could not be accounted for by upper bound type analysis.[16]

When FIDAP was used on this example, it clearly gave the buckling which was found experimentally. Figures 7 (a) and (b) show the mesh (for half the ring) at about 19·3 per cent reduction in height for cold and hot conditions. An iteration acceleration factor of 0·45 was used for the hot conditions, and 0·15 for the cold conditions, and threshold velocity for stress reduction

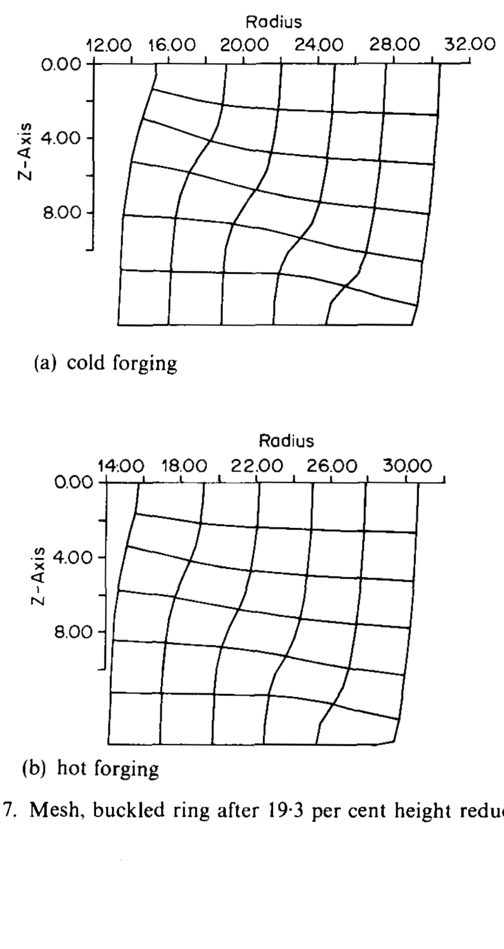

Figure 7. Mesh, buckled ring after 19·3 per cent height reduction

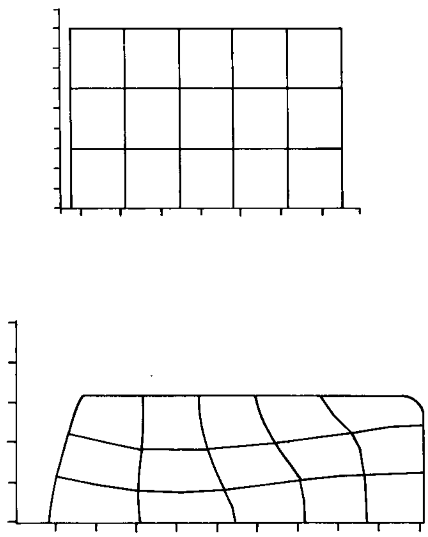

Figure 8. Thin specimen: cold forging; 29·5 per cent reduction

of 10 mm/s, but convergence was still not complete. Nevertheless, the result can be seen to compare well with the experimental result of Nagpai, Lahoti, and Altan.[14] The outer surface would be more rounded if compression were continued further but this would require renumbering and reconstructing of the mesh to allow for folding of free surfaces. (This will be the subject of another work).

Note. In all our examples we supposed the dye velocity constant. This was used to update the geometry. Thus if the dye velocity was V mm/s and the desired reduction per 'time step' was x per cent of initial height H, the current time increment would be (H/V) x per cent. This was used to compute the new geometry by moving all nodes from their current position by $u\Delta t$ where u is the flow 'velocity'.

CONCLUSIONS

In manufacture of parts for machinery, motors, vehicles and aircraft, a forming process is often used, in which hot metal is compressed between dies under high pressure. It is important to investigate details of what happens during the process, in order to optimize the conditions of pressure, shape of dies, and temperature for strongest, uniformly dense parts, of desired shape, and without faults, undue strains, or weak points. The FEM formulation of Bingham fluid flows does offer the requested model for the qualitative simulation of such processes. Use of standard programs such as FIDAP is possible provided one includes friction elements. For real-life die shapes one would have to include an automatic remeshing procedure.[17] Convergence of the quasilinear methods used here can be greatly improved by using Lagrange multipliers for the rigid zone constraints as similar to the methods given in Reference 18.

APPENDIX I—NOTATION

u_i—velocity component in the x_i direction
$u_{ij} = \partial u_i/\partial x_j$—partial derivative of u_i with respect to x_j

$\nabla u \equiv div\, u = \sum_i u_{i,i}$
D_{ij}—strain rate tensor components
σ_{ij}—stress tensor components
τ_{ij}—deviatoric stress tensor components
D_{II}—second invariant of strain rate tensor
τ_{II}—second invariant of deviatoric stress tensor
f_i—body force component per unit volume
μ—viscosity
ρ—density
g—yield limit (threshold of plasticity) for Bingham fluid
σ_0—yield stress in uniaxial tensile test
k—Von Mises criterion
Ω—Open domain in $\mathbb{R}^n$
Γ—boundary of Ω
m—friction factor
ε—penalty parameter
r, θ—cylindrical co-ordinates

APPENDIX II—FRICTION ELEMENT

Friction, as defined by the constant friction factor model, is in effect a tangential boundary stress, of value $m\sigma_0/\sqrt{3}$ directed against the motion of the boundary point, where m is the friction factor.

As with other applied surface stresses, it is necessary to calculate

$$\int_\Gamma \phi \bar{t}_i \,\mathrm{d}\Gamma = F_i \tag{73}$$

where ϕ is the velocity basis function, Γ is the boundary line, $\bar{t}_i$ is the applied stress vector in the x_i direction and F_i is the resultant force vector.

FIDAP defines a boundary velocity element to be used when it is desired to specify tangential or normal components of velocity or applied stresses on a boundary. The program will then premultiply by an orthogonal rotational matrix R and post-multiply by its transpose R^{T}, the stiffness matrix of any elements containing a node with the specified normal or tangential boundary condition (say node i), and premultiply by R the element force vector where

$$R = \begin{array}{cc} \begin{array}{ccccccc} & & j & & k & & \end{array} & \\ \begin{bmatrix} 1 & . & 0 & . & 0 & . & 0 \\ . & . & . & . & . & . & . \\ . & . & . & . & . & . & . \\ 0 & . & t_x & . & t_y & . & 0 \\ 0 & . & n_x & . & n_y & . & 0 \\ . & . & . & . & . & . & . \\ . & . & . & . & . & . & . \\ 0 & . & 0 & . & 0 & . & 1 \end{bmatrix} & \begin{array}{c} \\ \\ \\ j \\ k \\ \\ \\ \\ \end{array} \end{array}$$

j, k = position of x and y degrees of freedom in element stiffness matrix,
n_x, n_y = components of boundary normal at node i,
t_x, t_y = components of boundary tangent at node i.

This, in effect, transforms the x and y momentum equations for node i to t and n, tangential and normal degrees of freedom. Constrained values and stresses are treated accordingly. Since

$$\begin{aligned} u_n &= n_x u_x + n_y u_y, \\ u_t &= t_x u_x + t_y u_y, \qquad t = (-n_y, n_x), \end{aligned} \tag{74}$$

where u_n, u_t are the normal and tangential components of velocity, and u_x, u_y are the x and y components of velocity.

u_x and u_y can be recovered from (u_n, u_t) by

$$\begin{aligned} u_x &= n_x u_t - n_y u_n, \\ u_y &= n_y u_t + n_x u_n. \end{aligned} \tag{75}$$

Since friction is a tangential stress whose direction depends on tangential velocity, it was implemented into the boundary velocity elements.

Where friction is used, the program then forms the right hand side vector from

$$F_i = \int_\Gamma \frac{m\sigma_0 \phi}{\sqrt{3}} \mathrm{d}\Gamma. \tag{76}$$

$\sigma_0/\sqrt{3}$ is given by $g/\sqrt{2}$, where g is the yield stress for Bingham flow (see discussion following equation (14)).

The line integral is evaluated using

$$\mathrm{d}\Gamma = \left[\left(\frac{\partial x}{\partial s}\right)^2 + \left(\frac{\partial y}{\partial s}\right)^2\right]^{1/2} \mathrm{d}s, \tag{77}$$

where s is a parameter along the boundary, taking values from -1 to 1.

x and y are given by

$$x = N^{\mathrm{T}} \underset{\sim}{x}, \qquad y = N^{\mathrm{T}} \underset{\sim}{y}, \tag{78}$$

where $\underset{\sim}{x}$, $\underset{\sim}{y}$ are column vectors of nodal co-ordinates;

$$N = \begin{bmatrix} \frac{1}{2}s(s-1) \\ 1 - s^2 \\ \frac{1}{2}s(s+1) \end{bmatrix}$$

are the shape functions for an element boundary.

Hence

$$F_i = \int_{-1}^{1} \frac{mg\phi}{\sqrt{2}} \left[\left[\frac{\partial N^{\mathrm{T}}}{\partial s} \underset{\sim}{x}\right]^2 + \left[\frac{\partial N^{\mathrm{T}}}{\partial s} \underset{\sim}{y}\right]^2\right]^{1/2} \mathrm{d}s. \tag{79}$$

This integration is performed numerically by Gaussian quadrature using the value of the shape functions and derivatives given by the boundary velocity element.

When there were problems in obtaining convergent solutions for cases of high friction, a further development was made in the friction element to help convergence. Oh, Lahoti and Altan mention in their paper[3] that a smooth transition in the stress change near the neutral point was used. The formulation described so far leads to a very sudden change. Hence an additional parameter was introduced. Let us call that threshold parameter ε, and v_{T} the tangential velocity then we multiply (79) by $|v_{\mathrm{T}}|/\varepsilon$ if $|v_{\mathrm{T}}| < \varepsilon$.

REFERENCES

1. C. H. Lee and S. Kobayashi, 'Analysis of axisymmetric upsetting and plane strain side pressing of solid cylinders by finite element methods', *Trans ASME, Journal of Eng. Ind.*, **93,** 445 (1971).
2. O. C. Zienkiewicz and P. N. Godbole, 'Flow of plastic and visco-plastic solids with special reference to extrusion and forming processes', *Int. j. numer. methods eng.*, **8,** 3–16 (1974).
3. S. I. Oh, G. D. Lahoti and T. Altan, 'ALPID—a general purpose FEM program for metal forming', *Proc. 9th North Am. Manufacturing Res. Conf.*, University Park, PA, 1981, p. 83– 88.
4. S. I. Oh, G. D. Lahoti and T. Altan, 'Application of FEM to industrial metal forming processes', *Int. Conf. on Numeric Methods in Ind. Forming Processes*, Swansea, England, 1982.
5. M. S. Engelman, R. L. Sani, P. Gresho and M. Bercovier, 'Consistent vs. reduced integration penalty methods for incompressible media using several old and new elements', *Int. j. numer. methods fluids*, **2,** 25–42 (1982).
6. M. Fortin, 'Old and new finite elements for incompressible flows', *Int. j. numer. methods fluid*, **1,** 347–366 (1981).
7. M. Engelman, *FIDAP—Fluid Dynamics Analysis Program*, Theoretical and Users Manuals (revised Dec. 1982), FDI, Evanston, Illinois.
8. M. Bercovier, M. S. Engelman and M. Fortin, 'A finite element method for Bingham fluid flows', in D. H. Norrie (ed.) *3rd Int. Conf. on FE. in Flow Problems*, Banff, Alberta, Canada, 1980.
9. G. Duvaut and J. L. Lions, *Inequalities in Mechanics and Physics*, Springer-Verlag, 1976.
10. P. Hartley, C. E. M. Sturgers and G. W. Rowe, 'Friction in finite element analysis of metal forming processes', *Int. J. Mech. Sci.*, **21,** 301–311 (1979).
11. M. Bercovier, 'Approximation of Bingham's variational inequalities by a penalty function for the incompressibility constraint', *Numer. Func. Anal. and Optimize*, **2**(5), 361–373 (1980).
12. M. Bercovier and M. Engelman, 'A finite element method for incompressible non-Newtonian flows', *J. Comput. Phys.*, **36,** 313–326 (1980).
13. O. A. Ladyzenskaya, *The Mathematical Theory of Viscous Incompressible Flow*, Gordon and Breach, NY, 1964.
14. V. Nagpai, G. D. Lahoti and T. Altan, 'A numerical method for simultaneous prediction of metal flow and temperatures in upset forming of rings', *J. Engineering for Industry, Trans. ASME*, **100,** 413–420 (1978).
15. *Metals Handbook* (Ninth edn.), American Society for Metals, Metals Park, Ohio, 1978.
16. B. Abitzur, *Metal Forming Processes and Analysis*, McGraw Hill, 1968.
17. A. Badawy, S. I. Oh and T. Altan, 'A remeshing technique for the FEM simulation of metal forming processes', *Proc. 1983 Int. Computers in Eng. Cnf., Vol. I: CAD, Manufacturing and Simulation*, p. 143.
18. P. Tanguy, M. Fortin and L. Choplin, 'Finite element simulation of dip coating II: non-Newtonian fluids', *Int. j. numer. methods fluids*, **4,** 459–476 (1984).
19. M. S. Engelman, R. Sani and P. M. Gresho, 'The simplementation of normal and/or tangential boundary conditions in finite element codes for incompressible fluid flows', *Int. j. numer. methods fluids*, **2,** 225–238 (1982).